DALTON
FULL PAPER

Cascade chemistry in azacryptand cages: bridging carbonates and methylcarbonates †

Yann Dussart,[a] Charlie Harding,[a] Pia Dalgaard,[b] Christine McKenzie,[b] Renuka Kadirvelraj,[c] Vickie McKee[d] and Jane Nelson[e]

[a] *Chemistry Dept, Open University, Milton Keynes, MK7 6AA*
[b] *Kemisk Institut, University of Odense, Denmark*
[c] *Chemistry Department, University of Canterbury, Christchurch, New Zealand*
[d] *Chemistry Dept, University of Loughborough, UK, LE 11 3TU*
[e] *School of Biomedical Sciences, University of Ulster, Coleraine, UK BT52 1SA*

Received 14th November 2001, Accepted 19th February 2002
First published as an Advance Article on the web 20th March 2002

The different tendencies of dinuclear azacryptates of the *m*-$CH_2C_6H_4CH_2$ and 2,5-furano-spaced hosts L^1 and L^2 to catalyse CO_2 uptake-reactions within these sterically-protected host cavities are examined. Bridging methylcarbonates are generated catalytically upon exposure of methanol solutions of L^1, but not L^2, di-transition cation cryptates to atmospheric CO_2. X-Ray crystallographic structures of homodinuclear μ-carbonato cryptates of both ligands and μ-methylcarbonato cryptates of L^1 with later first transition series cations are reported. ESI-MS spectra show loss of H_2CO_3 from μ-carbonato cryptates in collision activation experiments.

The oxo-anion, carbonate, currently attracts attention in diverse areas of chemistry. Transformations involving this species, its reaction precursors and products are of considerable biological[1] significance; particularly important here are the carboanhydrases which play an essential role in processes such as photosynthesis, respiration, calcification and pH control. In the light of increasing concern about CO_2 build-up from fossil fuel consumption and potential resulting greenhouse effects, improved understanding of the biological handling of carbonate-related species acquires increasing urgency. Any potential new application of CO_2 as feedstock in chemical processes, will for this reason, attract much interest. In addition, the many and varied coordination modes of the carbonate oxo-anion are of spectroscopic interest as is their capacity to transmit magnetic interaction.[2–4] The carbonate system is also significant in the context of anion coordination chemistry as its behaviour within small molecule hosts may help to elucidate details of transport and location of carbonate or carboxylate anions in enzyme processes.

The frequently used strategy of anion coordination *via* protonated amine,[5,6] or other acidic host, can be problematic in such pH-sensitive systems, so we have adopted an alternative strategy: the oxoanions here are retained *via* their bridging coordination of cations held within a cryptand cavity. We have already used the "cryptate as host" strategy to coordinate pseudo-halide anions such as azide and cyanate, and studied the spectroscopy and magnetochemistry[7,8] resulting from the consequent (and on first observation unprecedented) colinear M–NXY–M bridging geometry.

The secondary coordination of anionic or other bridges between cations themselves coordinated by a cryptand host molecule was quite some time ago termed *cascade* coordination by Jean-Marie Lehn,[9] in the implicit expectation that the bridging groups might be activated, by reason of their dicoordination, toward further and possibly useful chemical reaction. However, such outcome was not apparent in our pseudo-halide series despite physical and spectroscopic properties quite distinct from those seen in ionic, terminal or "normal geometry" dicoordinated modes. Nonethless we thought it worthwhile to extend the study to more labile systems such as carbonate. Functionalization of carbonate, for example, to generate carbonate esters of value to the polymer industry would be an attractive target, given the need for development of safer synthetic methods.[10]

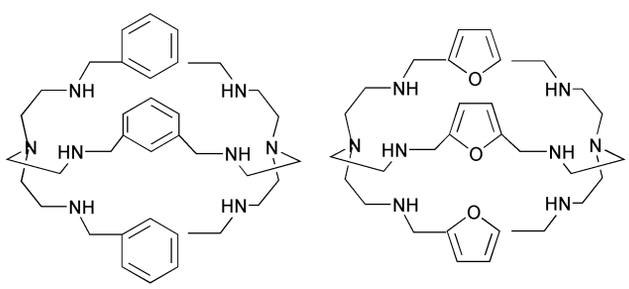

L^1 L^2

Dinuclear transition ion complexes of the azacryptand hosts, L^1 and L^2, which have the capacity[7,8,11] to operate as receptors for pseudo-halide anions (and other oxo-anions[12]) were used in this study. We used these precursors *in situ* to synthesise carbonato-bridged cascade complexes, and examine their structures. We also wished to examine spectroscopic and magnetochemical properties which might reveal any correlation of these properties with the mode of bridging adopted. Two main classes of compound emphasised in this study are carbonato-bridged azacryptates and the methylcarbonato-bridged derivatives which result from catalytic reactions described in later sections.

Results and discussion

The cascade carbonate complexes (Table 1) were generated directly by treatment of the free cryptand with the appropriate cation salt and bridging anion in appropriate stoichiometry. In

† Electronic supplementary information (ESI) available: magnetic data. See http://www.rsc.org/suppdata/dt/b1/b110449g/

 DOI: 10.1039/b110449g

Table 1 Analytical and selected spectroscopic for the carbonato and methylcarbonato-bridged cryptates

Cryptate	C; H; N Analytical data: found (calc.)	Carbonate IR peaks/cm^{-1}	ESMS base peak
$[Cu_2L^1(CO_3)](ClO_4)_2\cdot 2H_2O$ **1**	43.5(43.7); 5.7(5.7); 10.9(11.0)	1449ms,[b] 1417ms,[b] 830mw	392.2
$[Cu_2L^1(MeCO_3)](ClO_4)_3\cdot 4H_2O$ **2**[d]	38.6(39.3); 5.1(5.6); 9.6(9.6)	1635s, 1345m	450.1
$[Ni_2L^1(CO_3)](ClO_4)_2\cdot 2H_2O\cdot 2MeOH$ **3**[d]	43.3(43.5); 5.6(5.8); 10.7(10.4)	1483ms,[b] 1453ms,[b] 836mw	387.1
$[Ni_2L^1(MeCO_3)](ClO_4)_3\cdot 4H_2O$ **4**[d]	38.8(39.6); 5.7(5.7); 10.2(9.7)	1673s, 1368mw	—[a]
$Co_2L^1(CO_3)(ClO_4)_2\cdot 2H_2O$ **5**	44.0(43.9); 5.8(5.8); 10.6(11.1)	1478s,[b] 1456ms,[b] 836mw	388.1
$[Co_2L^1(MeCO_3)](ClO_4)_3\cdot 4H_2O$ **6**	39.1(39.3); 5.4(5.3); 9.6(9.7)	1637s, 1345mw	445.2
$[Ni_2L^2(CO_3)](ClO_4)_2$ **7**	39.4(39.4); 5.1(5.1); 11.1(11.8)	1528ms, 1378mw,[b] 837mw	373.2
$[Co_2L^2(CO_3)](ClO_4)_2$ **8**[d]	39.4(39.4); 5.1(5.1); 11.7(11.8)	1534ms, 1370ms,[b] 839mw	373.0
$[Zn_2L^2(CO_3)](ClO_4)_2$ **9**	38.9(38.9); 5.2(5.0); 11.7(11.7)	1492ms,[b] 1437ms,[b] 1360sh,[b] 841mw	378.9
$[Zn_2L^1(MeCO_3)](ClO_4)_3\cdot 2H_2O$ **10**[d]	40.1(39.8); 5.3(5.3); 9.9(9.7)	1643s, 1337m	442.2
$[Zn_2L^1(CO_3)](ClO_4)_2\cdot 3H_2O$ **11**	[c]	1478ms,[b] 1453ms,[b] 1430ms 946mw, 838mw	394.2

[a] ESMS unobtainable. [b] Assignment uncertain due to overlapping with ligand peaks. [c] Acceptable analysis not obtained for bulk sample. [d] Solvation in bulk sample differs from that in crystals used for X-ray diffraction.

both cryptand systems, carbonate and hydrogencarbonate appear to act interchangeably.

Direct treatment of an ethanolic solution of L^1 and metal salt in 1 : 2 stoichiometry with 1 equivalent of anion followed by recrystallisation from acetonitrile led to isolation of the μ-carbonato complex, while the outcome of such treatment in a methanol solvent led instead to isolation of a η^1,η^1 μ-methylcarbonate derivative. However with L^2 the nature of the complex isolated did not depend on the solvent used: μ-carbonato cryptates were obtained with dicobalt, dinickel and dizinc systems in both ethanol and methanol solvents.

X-Ray structures

Carbonato-bridged structures. Structures of bridged carbonato cryptates were obtained for dicopper(II), dinickel(II), dizinc(II) and dicobalt(II) complexes, in the last case for both ligands studied, L^1 and L^2. With all four cations, the oxo-anion bridges (*via* at least two of the O-donors) the encapsulated cations which are also coordinated by the three secondary amino donors and the tertiary nitrogen bridgehead of the host. Other conditions were not identical however, as cation coordination number alters across the series together with the mode of bridging. The *anti–anti* η_1,η_1 mode ***B*** (Scheme 1) was adopted

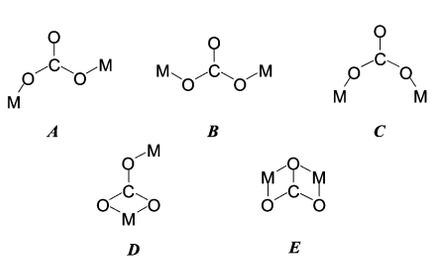

Scheme 1

in the dicopper **1** and dinickel **3** cryptates (see Table 1 for numerical codes) while the strategies used by cobalt in **5** and **8** were more complex, also involving the third carbonate O-donor in coordination with utilisation of modes ***D*** and ***E***. However it should be noted that even in **1** and **3** where cation coordination is restricted to two of the three carbonate O-donors, the third carbonate oxygen is engaged in hydrogen bonding to solvate molecules.

The only case where a *syn–anti* μ-η_1,η_1 mode ***A*** bridged carbonate derivative is isolated occurs in the dizinc L^1 system, as structure **11**, obtainable when methanol is absent. Thus all main modes of μ_2-carbonate bridging known to exist in isolation (*i.e.* excluding mode ***C*** which has so far been observed only as supporting bridge to another ligand such as μ-oxo or μ-hydroxo) are observed in this series of cryptates.

The dicopper cryptate $[Cu_2L^1(CO_3)](ClO_4)_2\cdot 2H_2O$, **1**, Fig. 1, shows a trigonal bipyramidal site for both coppers, with the

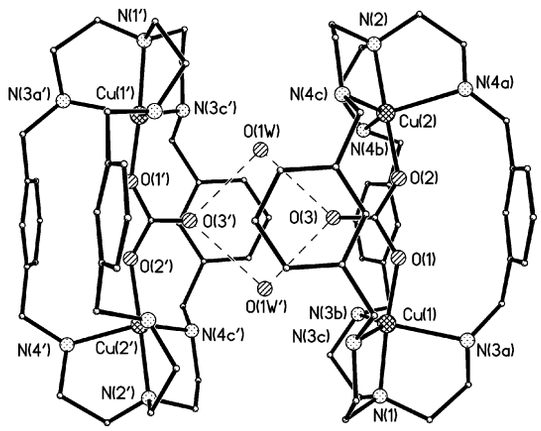

Fig. 1 Water-mediated hydrogen-bonding between two $[Cu_2L^1(CO_3)]^{2+}$ cations. Hydrogen-bond distances: O(3) ··· O(1W) 2.816(3), O(3) ··· O(1W′) 2.813(3) Å.

carbonate O-donor in the diaxial position, using the *anti–anti* bridging mode. The mean of the equatorial Cu–N distances (Table 2) is 2.146 Å and those of the axial Cu–N_{br} and Cu–O, 2.040 and 1.873 Å, respectively. The OCO angle in the bridge is 113.7(3)°. One of the water molecules hydrogen-bonds the uncoordinated carbonate oxygens of a pair of cryptates, generating a hydrogen-bonded dimer held together by a pair of bridging water molecules, as shown in Fig. 1. The intercryptate Cu ··· Cu distance is 6.785(1) Å compared with an intracryptate Cu ··· Cu separation of 5.7911(8) Å.

The dinickel analogue $[Ni_2L^1(CO_3)(MeOH)_2](ClO_4)_2\cdot 2H_2O$, **3**, Fig. 2, exhibits the same *anti–anti* bridging mode as **1**, but

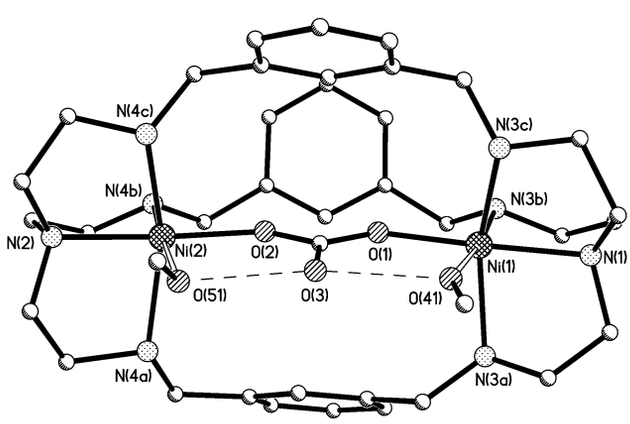

Fig. 2 The $[Ni_2L^1(CO_3)(MeOH)_2]^{2+}$ cation. Hydrogen-bond distances: O(3) ··· O(41) 2.55(1), O(3) ··· O(51) 2.51(1) Å.

here the nickel cations have each achieved their preferred six-coordination by coordinating a molecule of methanol solvent. The uncoordinated O-donor of the carbonate bridge is once

Table 2 Selected bond lengths (Å) and angles (°)

	1	2	3	4[a]	5a	5b	8	10[a]	11
M–O	1.872(2)	1.941(3)	1.946(7)	2.010(10)	1.904(6)	1.951(6)	2.145(9)	2.061(4)	1.979(2)
	1.875(2)	1.963(3)	1.969(7)	2.049(12)	1.920(6)	2.208(6)	2.146(9)	2.099(4)	1.989(2)
						2.024(6)	2.151(9)		
							2.157(9)		
M–N(br)	2.032(3)	2.034(3)	2.081(11)	2.084(8)	2.191(8)	2.139(7)	2.177(10)	2.279(5)	2.232(3)
	2.048(3)	2.040(3)	2.106(10)	2.085(8)	2.193(8)	2.281(7)	2.180(11)	2.291(5)	2.268(4)
M–N(strand)	2.105(3)	2.061(3)	2.126(8)	2.032(14)	2.11(2)	2.088(7)	2.165(12)	2.138(5)	2.095(3)
	2.116(3)	2.074(3)	2.126(8)	2.081(8)	2.127(7)	2.099(8)	2.236(10)	2.152(5)	2.178(3)
	2.216(3)	2.232(3)	2.151(8)	2.139(8)	2.161(7)	2.138(10)	2.261(11)	2.192(6)	2.188(3)
	2.090(3)	2.034(3)	2.124(9)	2.088(16)	2.123(8)	2.212(7)	2.154(12)	2.117(5)	2.100(3)
	2.120(3)	2.086(3)	2.136(9)	2.102(8)	2.148(7)	2.229(7)	2.205(10)	2.155(5)	2.137(3)
	2.227(3)	2.158(3)	2.243(10)	2.121(8)	2.158(7)	2.244(8)	2.247(10)	2.168(4)	2.159(3)
M–X			2.202(8)		2.40(2)				
			2.445(8)		2.604 (11)				
M(1)–M(2)	5.7911(8)	5.6554(6)	6.018(2)	5.6287(18)	5.9389(16)	5.1291(17)	4.2924(3)	5.9817(9)	5.3308(6)
M–O–C	135.3(2)	151.9(3)	140.3(7)	141.1(10)	141.4(6)	128.3(6)	90.0(8)	125.6(3)	133.6(2)
	131.5(2)	120.3(2)	137.7(6)	121.1(8)	139.6(5)	86.2(5)	90.7(8)	154.5(4)	120.2(2)
						93.9(5)	92.4(9)		
							93.3(8)		

[a] Data given for the major component of disorder. [b] X = O from MeOH (**3**) or H_2O (**5**).

more hydrogen-bonded, this time to the pair of methanol solvate molecules. It is notable that, while the hydrogen bonds are quite strong, the Ni–methanol distances are long (Table 2), suggesting that the hydrogen-bond may be the more significant interaction. The Ni–N and Ni–$O_{carbonate}$ distances (Table 2) average at ≈ 2.15 Å and ≈ 1.96 Å, respectively, and in contrast to the dicopper analogue, the intramolecular nature of the hydrogen bonding leaves each Ni cryptate magnetically isolated within the structure. In consequence of the longer M–N_{br} (by ≈ 0.05 Å) and M–O (by ≈ 0.07 Å) distances the M ··· M internuclear separation of 6.018(2) Å is the longest in the series.

The dicobalt complex, **5**, effectively the dimer $[Co_2(L^1)(CO_3)][Co_2(L^1)(CO_3)(H_2O)_2](ClO_4)_4{\cdot}2H_2O$ crystallises with two independent cations of different structure in the asymmetric unit. One cation exhibits the *anti–anti* μ-η_1,η_1 carbonato-bridged structure seen in **1** and **3**; as with the dinickel analogue the uncoordinated oxygen atom of the carbonate group is strongly hydrogen-bonded to two solvate molecules which are also weakly coordinated to the metal ions (Fig. 3(a), Table 2). The second cation shows the μ-η_1,η_2 variant in which all three carbonate O-donors are coordinated (Fig. 3(b)). One cobalt ion, Co(3), is five-coordinate with approximate trigonal bipyramidal geometry while Co(4) is six-coordinate. A further consequence of the alteration in bonding mode is to bring the cobalt ions considerably closer together (Co(1) ··· Co(2) 5.939(2), Co(3) ··· Co(4) 5.129(2) Å).

The dizinc analogue $[Zn_2(L^1)(CO_3)](ClO_4)_2{\cdot}6.5H_2O$ (**11**) adopts a structure intermediate between the two shown in complex **5**: the *syn–anti* mode (Fig. 4). This cryptate shows slightly larger M–O and M–N_{br} distances than the mode ***B*** bridged carbonates, which may be due to the larger effective radius of the Zn(II) cation. The shorter internuclear M ··· M separation in **11** *vs.* **5a** is a consequence of the alteration of the mode of carbonate binding.

The dicobalt(II) cryptate of the furano-linked host L^2: $[Co_2L^2(CO_3)](ClO_4)_2{\cdot}2H_2O$, **8**, Fig. 5, uses a more radical approach to the challenge of utilising all three carbonate O-donors by adopting the μ-η_2,η_2 bridging mode. While this results in M–O-donor distances longer by ≈ 0.3 to 0.1 Å than elsewhere in the carbonate series, as well as somewhat longer (by ≈ up to 0.15 Å) M–N bonds, the M ··· M distance, at (4.2924(3) Å) is markedly shorter than for any carbonato-bridged complex of the L^1 cryptand. The shorter cavity in L^2 encourages this more compact arrangement.

The relatively high magnetic coupling constant (*q.v.*) observed in the dinickel analogue **7**, which has not been structurally characterised, strongly suggests that the μ-η_2,η_2 bridging

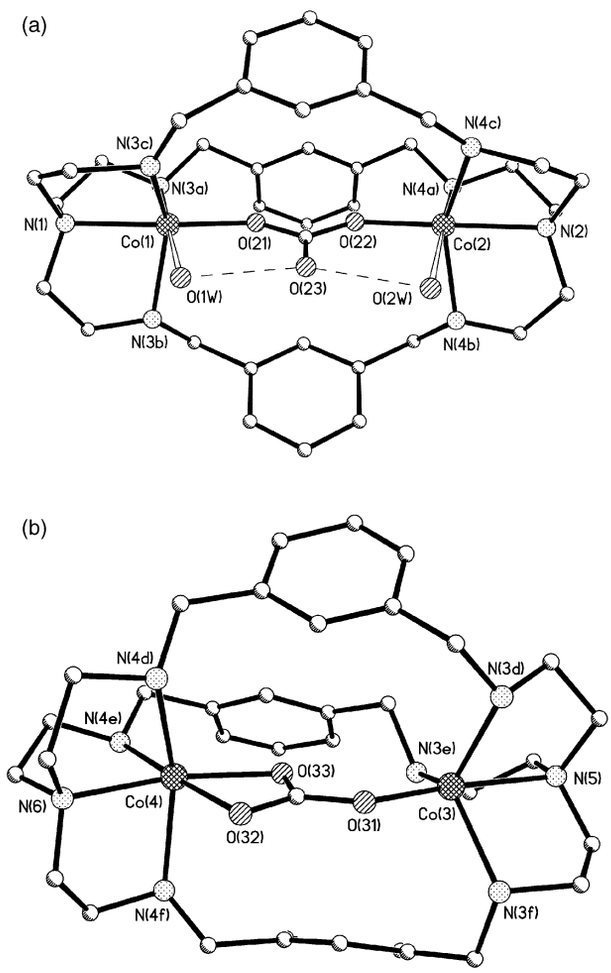

Fig. 3 (a) The symmetric cation of **5**: hydrogen-bond distances 2.54(2) and 2.57(1) Å for O(23) to O(1W) and O(2W), respectively. (b) The asymmetric cation: Co(3)–O(31) 1.951(6), Co(4)–O(32) 2.028(6), Co(4)–O(33) 2.024(6) Å.

mode is also adopted in this cryptate. This is not surprising given the preference of the Ni(II) cation for six-coordination. A dizinc analogue **9**, also structurally uncharacterised, shows an IR spectrum similar to **7** and **8** though with carbonate ν_3 IR absorption at somewhat lower frequencies (by 30–40 cm^{-1}), so its coordination mode is uncertain. The absence of solvation does suggest that all carbonate O-donors are utilised in

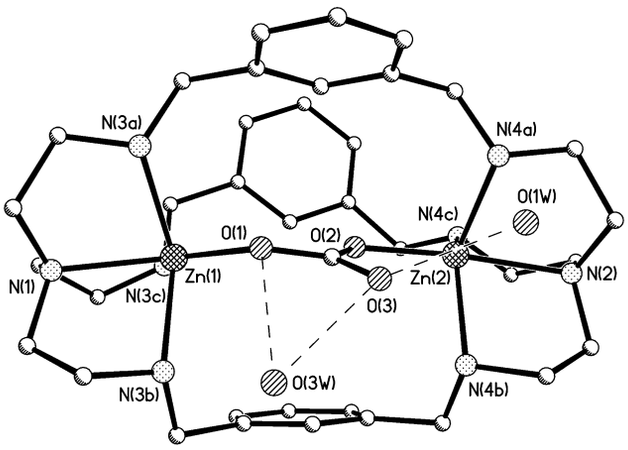

Fig. 4 The $[Zn_2(L^1)(CO_3)]^{2+}$ cation. Hydrogen-bond distances: O(1W)–O(3) 2.697(4), O(3W)–O(1) 3.098(4), O(3W)–O(3) 2.812(4) Å.

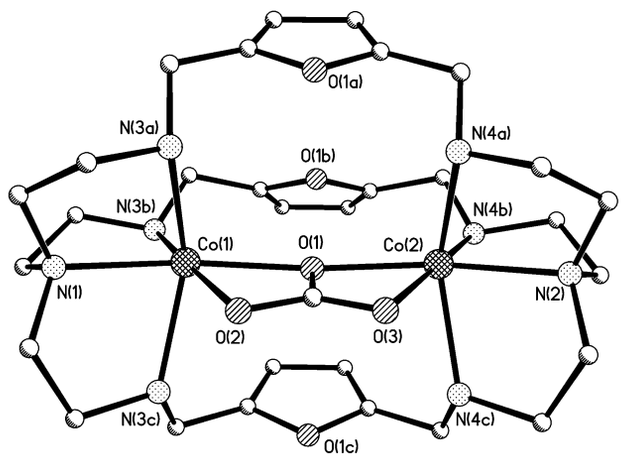

Fig. 5 The $[Co_2L^2(CO_3)]^{2+}$ cation.

coordination, possibly *via* an unsymmetric[13] variant of mode ***E*** coordination. An attempt to generate the dicopper(II) carbonato-bridged cryptate of L^2 by treatment of preformed carbonate with $[Cu_2L^2]^{2+}$ failed, yielding instead an impure sample of the known[14] linear μ-hydroxo bridged analogue. Overall, these results confirm the preference of L^2 cryptates for monatomic or effectively monatomic bridging arrangements such as μ-η_2,η_2.

All of the structures discussed above show extensive hydrogen-bonding through the lattice involving the cryptate amines, anions and solvate molecules. Details of these interactions can be found in the supplementary data (supplied as CIF, see footnote in the Experimental section).

The rich variety of coordination modes adopted in this series of carbonato-bridged complexes is reminiscent of those adopted in the carboxylate series, which exemplify stages in the *carboxylate shift* mechanism utilised by μ-carboxylato manganese and iron proteins, to allow alteration of cation coordination number and geometry *via* a low energy route.[15,16] The carbonate geometries analogous to stages in the carboxylate shift mechanism are illustrated in Scheme 2, together with the modes to which they relate. The existence of modes ***B*** and ***D*** in the same crystal in **5** suggests that no more than small energy differences exist between these bridging modes in the carbonate system.

Methylcarbonato-bridged structures generated by CO_2 fixation. Although the reaction of CO_2 with hydroxide to generate hydrogencarbonate or carbonate ion is extremely slow in the absence of catalysis, there have been many examples of uptake of CO_2 followed by catalysis of this reaction in dinuclear transition ion systems.[13,17,18] We thus attempted synthesis of carbonato-bridged cryptates without deliberate addition of the oxo-anions to see if CO_2 uptake would provide the bridging anion. We did not obtain μ-carbonato complexes in a pure form *via* this route; both IR and mass spectrometric evidence suggest contamination by hydrogencarbonate and/or hydroxo complexes, particularly evident when the synthesis was not carried out under CO_2 atmosphere. In methanol solution, however, the catalytic strategy was dramatically successful in the L^1 series, generating, even under ambient atmospheric conditions, the methylcarbonato-bridged cryptates discussed below.

In the synthesis of these methylcarbonato derivatives, two alternative synthetic procedures (which may indeed generate the same reaction) were used.

(i) Treatment of a methanol–acetonitrile solution of a 1 : 2 cryptand–cation mixture under aerobic conditions with one equivalent of preformed carbonate anion, HCO_3^- or CO_3^{2-}.

(ii) *in situ* reaction of coordinated methoxo ligand with atmospheric CO_2.

Identical products were obtained irrespective of whether procedure (i) or (ii) was used. Recognition of the existence of this catalytic reaction resolved our earlier puzzlement about why a linear μ-hydroxodicopper(II) cryptate analogous to that[14] of L^2 was not obtained when L^1 was treated[19] with Cu(II) in methanol solution under ambient conditions (effectively synthetic procedure (ii)). The explanation is that, consequent upon efficient catalysis of the CO_2 absorption reaction by dicopper(II) coordinated within the L^1 cavity, the product obtained was the methylcarbonato-bridged cryptate instead of the expected μ-hydroxodicopper(II) analogue.

Crystals of **2**, **4** and **10** obtainable by both methods (i) and (ii), showed very similar structures, indicating a preference for the *syn–anti* μ-η_1,η_1 mode ***A*** (Fig. 6). The dicopper structure is ordered while the dinickel and dizinc analogues both show disorder of the methylcarbonate anion between the two equivalent *syn–anti* arrangements within the cavity. Given the similarity of the three cation structures, it is noteworthy that the metal–metal distance is significantly longer in the dizinc complex, **10**, (Table 2).

In comparison with the carbonate structures discussed earlier, the only well defined differences, *vs.* the mode ***B*** carbonates **1**, **3** and **5**, are the marginally significant decrease in average M–N distance (by ≈ 0.05 Å) and a more significant contraction of the M ··· M internuclear separation (by ≈ 0.15–0.4 Å). No such effect is evident when comparing the dizinc μ-methylcarbonato cryptate **10** with its μ-carbonato analogue **11**, as mode ***A*** coordination of the O–C–O moiety is utilised in both cases.

The CO_2 insertion reaction is relatively rapid for dizinc and dicopper precursors (crystals of **2** and **10** may be isolated within hours standing in air) while with dicobalt and dinickel precursors more than a day is required for isolation of the methylcarbonate product; in fact for the dinickel complex **4** the mid blue crystals are often to some extent contaminated with a paler impurity. Isolation of a MeOH solvate of a carbonato- rather

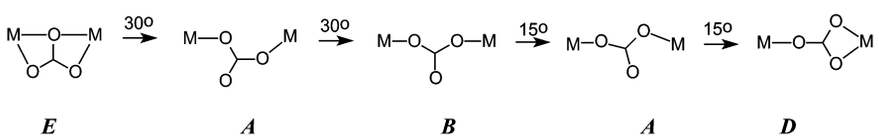

Scheme 2

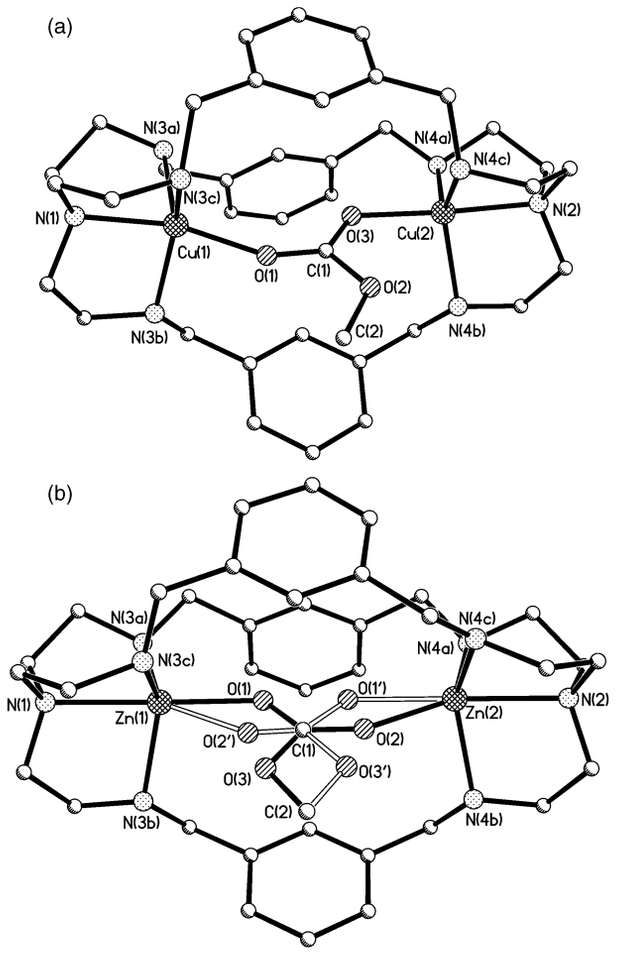

Fig. 6 (a) Structure of the $[Cu_2(L^1)(MeCO_3)]^{3+}$ cation. (b) The $[Zn_2(L^1)(MeCO_3)]^{3+}$ cation showing disorder of the methylcarbonate group; similar disorder is present in the structure of the nickel analogue.

than a methylcarbonato complex when **3** is recrystallised from MeCN–MeOH under aerobic conditions indeed testifies to a relatively slow rate of CO_2 reaction where the cation is Ni(II).

There are few well-substantiated examples of CO_2 insertion into O–R bonds, and mechanistic studies of this reaction have yet to be undertaken. Other workers[20] have assumed a mechanism analogous to that for hydrogencarbonate[21] formation, *i.e.* initial coordination of solvent methanol which deprotonates, followed by nucleophilic attack of coordinated methoxo on CO_2; effectively an insertion of CO_2 into the M–OMe^- bond. The host L^1 (in comparison with L^2) is particularly effective in promoting this reaction. Within the L^2 system, with its shorter cavity, we have demonstrated[14,22] ready encapsulation of μ_2-hydroxo as a tightly coordinated bridge; formation of an analogous μ_2-alkoxo complex presumably terminates the catalytic cycle by blocking the insertion reaction. Transient monodentate coordination of alkoxo within the longer L^1 cavity on the other hand seems a feasible option, presenting a viable route to methyl carbonate formation. The fact that the strongest Lewis acid Zn(II) is much the most effective cation in the catalytic process supports the hypothesis of methanol deprotonation as the rate-determining step. A similar mechanism has been invoked by Mingos and coworkers[20] to explain the isolation of alkylcarbonates from magnesium alkoxides in the presence of CO_2.

No evidence has been obtained for $MeCO_3^-$ generation *via* CO_2 uptake by dinuclear assemblies held within the L^2 host. When a nickel salt was allowed to stand in air over several days with the stoichiometric amount of cryptand in MeOH–MeCN solution, no crystallisation of μ-methylcarbonato- or μ-carbonato cryptate was observed, but crystallisation of **7** ensued in good yield within hours of the addition of a stoichiometric amount of preformed carbonate ion.

Spectroscopic properties

Because of the comprehensive X-ray structural data available we attempted (Table 1) to correlate IR C–O stretching frequencies with the mode of bridging adopted. Although the significant degree of overlap between carbonate and cryptand or counter-ion absorptions hindered this attempt, the spectral features asociated with different carbonate coordination modes were internally consistent and an aid to their recognition. The asymmetric stretching mode, ν_3, of the carbonate ion, seen as a strong absorption around 1450 cm^{-1} in the free ion, is split to some extent in the dicoordinating η^1,η^1 μ-carbonato situation and appears as two or more components in the range 1400–1500 cm^{-1}, which overlap with moderately strong cryptand skeletal modes centred about 1440–1480 cm^{-1}, preventing unambiguous assignments. We can also frequently recognise the out-of-plane bending mode, ν_2, as a moderately weak sharp absorption near 840 cm^{-1}. These frequencies are typical of ν_3 and ν_2 absorptions in dinuclear bridged carbonates.[23] Both intensity and frequency of the asymmetric stretch ν_3 make it the most useful characteristic frequency of carbonate. The weaker in-plane bend, ν_4, seen near 700 cm^{-1} in the free ion, and the symmetric stretch, ν_1, IR-forbidden in the free ion, may not be reliably assigned because of the presence of more intense cryptand or counter-ion absorptions.

For the η^1,η^1 μ-methylcarbonato complexes, the effect of esterification of one of the carbonate bonds, generating a strongly covalent O–Me single bond, is to increase the bond order in the remaining C–O bonds.[23–25] The series of η^1,η^1 alkylcarbonate complexes of magnesium isopropoxide systems which have recently been structurally and spectroscopically characterised[20] show IR absorptions in similar spectral ranges. The non-methylated CO bonds generate ν_{as} OCO absorption which appears at significantly higher frequency (above 1600 cm^{-1}) than does that of the esterified C–O bond, with a separation between these absorptions of ≈ 300 cm^{-1}. The μ-methylcarbonato ν_{as} OCO frequency is similar to those seen for μ-carboxylates[26] where the OCO oscillator likewise shows enhanced bond order compared to analogous carbonate-bridged systems.

The μ-η_2,η_2 bridging mode ***E*** present in **8** and **7** is also associated with increase of ν_{as} OCO above that seen in the η^1,η^1 *anti–anti* bridging mode ***B***: a slight but consistent increase in wavenumber of the sharp absorption which consequently appears close to or above 1500 cm^{-1} is indicative of this mode.

Magnetic interactions

Of the twelve modes of coordination of the carbonate ligand,[27] the five that are known in dinuclear complexes, illustrated in Scheme 1, show a range of ability to mediate magnetic exchange. Relevant here are modes ***A*** (weak *anti*ferromagnetic to ferromagnetic), ***B*** (moderate to weak antiferromagnetic), ***D*** (weak antiferromagnetic) and ***E*** (strong antiferromagnetic). In the following discussion, coupling constants are defined as J as in eqns. (1) and (2) (Experimental section) as are values quoted from other work

Carbonate-bridged complexes. As **1**, **3** and one pathway in **5** utilise the *anti–anti* η_1,η_1 bridging mode ***B***, albeit with variation of coordination of the dinuclear carbonate moiety, this series may be compared with previous studies of this mode of bridging. Within the *anti–anti* η_1,η_1 bridging mode (***B***), magnetic exchange is observed to be weak in nickel complexes,[28] and moderately antiferromagnetic in square-based copper complexes,[2] where coupling constants in the range 120–140 cm^{-1} are observed. The trigonal bipyramidal coordination in **1** evidently presents a more efficient exchange pathway ($-2J \approx 200$ cm^{-1},

Table 3 Magnetic data for dicopper(II) dinickel(II) and dicobalt(II) cryptates[c]

Cryptate	μ_{275}/μ_B	μ_{80}/μ_B	$-J/cm^{-1}$	g	TIP/10^{-6} cm^3mol^{-1}
$[Cu_2L^1(CO_3)](ClO_4)_2\cdot 2H_2O$ **1**[a]	1.50	0.81	210 ± 5	1.93 ± 0.01	60
$[Cu_2L^1(MeCO_3)](ClO_4)_3\cdot 4H_2O$ **2**	1.90	1.84	11 ± 1	2.17 ± 0.01	60
$[Ni_2L^1(CO_3)](ClO_4)_2\cdot 2H_2O\cdot 2MeOH$ **3**	2.82	2.56	1.9 ± 0.2	2.10 ± 0.01	200
$[Ni_2L^1(MeCO_3)](ClO_4)_3\cdot 4H_2O$ **4**	3.09	2.84	10.1 ± 0.1	2.15 ± 0.01	200
$Co_2L^1(CO_3)(ClO_4)_2\cdot 2H_2O$ **5**	4.48	4.18	2.8 ± 0.1	2.27 ± 0.01	200
			11 ± 1	2.40 ± 0.01	
$[Co_2L^1(MeCO_3)](ClO_4)_3\cdot 4H_2O$ **6**	4.39	4.27	1.4 ± 0.1	2.19 ± 0.01	400
$[Ni_2L^2(CO_3)](ClO_4)_2$ **7**[a]	2.41	1.26	108 ± 1	1.97 ± 0.01	500
$[Co_2L^2(CO_3)](ClO_4)_2$ **8**[b]	4.24	2.98	30 ± 1	2.35 ± 0.01	500

[a] For complexes **1** and **7** a paramagnetic impurity term evaluated as 6% for **1** and 1.8% for **7**. [b] Parameters derived from data in the range 70–280 K as described in Experimental section. [c] Per M^{2+} ion.

Table 3) resulting from favourable alignment of the magnetic d_{z^2} orbital towards the a_2' carbonate molecular orbital. By contrast, the low J value of the dinickel complex **3** is in good agreement with previous studies of the *anti–anti* η_1,η_1 bridging mode ($J = -4.6$ cm^{-1}) in nickel complexes,[28] even though in **3** the intervention of hydrogen-bonded methanol may be expected to draw electron density from the carbonate bridge. We assume that mode ***B*** mediates the stronger of the two exchange paths in **5** (see Experimental section). As expected, the J value (-11 cm^{-1}) is considerably lower than that observed when a third oxygen of the carbonate provides an additional monatomic bridging pathway as in mode ***E*** (see discussion of complex **8** below), but no similar examples of mode ***B*** are known in cobalt complexes.

For the alternate mode ***D*** pathway of **5**, the interaction is as expected significantly lower, as the *syn–anti* component of the pathway is normally weak, sometimes even ferromagnetic in sense, leading to reduction or approximate cancellation of the *anti–anti* component.[29]

The μ-η_2,η_2 mode ***E*** adopted in **7** and **8** is normally associated with relatively strong interaction, according to the predictions of extended Huckel theory.[2,30] In examples of dinuclear[18] and several polynuclear Ni(II) complexes,[31] in which this bridging mode predominates, $-2J$ values in the range 82–95 cm^{-1} have been reported. The coupling appears to correlate with the Ni–O–Ni angle although only a small range (172–174°) is available. Fig. 7 compares the effect on susceptibility of the dinickel

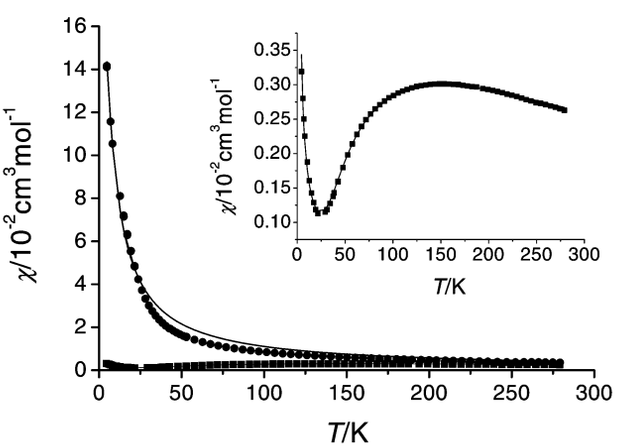

Fig. 7 Magnetic behaviour (χ *vs.* T) for complexes **3** (circles) and **7** (squares) showing the contrasting exchange coupling of dinickel μ-carbonato complexes of ligands L^1 (mode ***B***) and L^2 (mode ***E***). The lines show the fit of χ as a function of T corresponding to eqn. (1) with parameters in Table 3. The inset graph shows the behaviour of **7** on an appropriate scale.

systems of mode ***E***-mediated interaction in **7** with mode ***B***-mediated interaction in **3**. For the one dicobalt(II) complex in which a μ-η_2,η_2 mode has been previously reported[32] (with Co–O–Co angle of 171°), the corresponding coupling constant is -20 cm^{-1}, significantly less than observed for complex **8** which has a larger Co–O–Co angle at 174.5°, consistent with the expected effect of M–O–M angle on the coupling.

Methylcarbonate-bridged complexes. Although there are no previous reports of magnetic exchange in *syn–anti* μ-η_1,η_1 methyl carbonates, the prediction of Hückel theory is that the intradimer interaction should be weak.[33] Comparison may be made with the behaviour of *syn–anti* carboxylate bridged systems, which have been studied in cluster and polymeric compounds[34] involving square pyramidal copper. These usually exhibit ferromagnetic coupling, although weak antiferromagnetic coupling has also been observed in a few instances. In the series **2**, **4** and **6**, exchange coupling is weak and, despite our expectation for complexes with closely similar coordination geometry, a dependence[35] of J on n^{-2} is not observed between dicopper (**2**) and dinickel (**4**) systems. Thus we infer that small changes in geometry are crucial in determining the magnitude of the interaction in this mode of bridging. The structure of complex **6** was not determined, but as far as we may imply from its magnetic behaviour, this complex has a similar bridging geometry to complex **2**, as evidenced by the constancy of the term n^2J in this pair of cryptates.

Electrospray ionisation (ESI) mass spectrometry

The developing technique of electrospray mass spectroscopy (ESI-MS) is in increasing use in inorganic chemistry to probe fragmentation patterns,[36] including those of carbonate oxoanions,[37] so we have studied the ESI-MS of the structurally characterised carbonato- and methylcarbonato-bridged cryptates.

A listing of the major ions observed in the ESI mass spectra of the carbonate can be found in Table 4. For L^1 cryptates both carbonate and hydrogen carbonate peaks were observed with substantial intensity suggesting that both species may be present in solution. Source conditions were varied but the results were not conclusive in determining gas- or solution-phase origin. However the peak intensities are consistent with the formulations of carbonate in the original solid samples. For example the $[LM(CO_3)]^{2+}$ ions are the base peaks for the solid carbonate compounds **1**, **3**, **5**, **8** and **11**. There is no clear evidence for the presence of hydrogencarbonato complexes in the solid state although the first crop obtained in the synthesis of the methylcarbonato-bridged dizinc L^1 cryptate **10** shows hydrogencarbonato-derived ions at relatively high intensity; the most prominent peaks being those due to hydrogencarbonate species $[LM(HCO_3)(ClO_4)_2]^+$ 989.3 and $LM(HCO_3)(ClO_4)]^{2+}$ (445).

The carbonate species were subjected to collision activation (CA) using Ar gas in MS/MS experiments in an attempt to glean structural information, *i.e.*, differences in stability that could be related to the various bonding modes of the bridging carbonate ligand (Scheme 1) or extent of carbonate proton-

Table 4 Ions observed (*m*/*z* value for the major isotopomer of the cluster) in the ESI mass spectra of the carbonate and bicarbonate complexes. Intensities obtained [a, b] using the same experimental conditions are given in parentheses. Ions produced by collision activation are listed under parent ions in italics (explanation in text)

Cryptate	**1**	**5**	**3**	**11**	**7b** [b]	**9b** [b]	**8**
$[LM(CO_3)]^{2+}$	392.2(100) *360.9*	388.1(100) *356.8*	387.1(100)	394.2(100)	373.2(100)	378.9(100)	373.0(100) *341.8*
$[LM(HCO_3)]^{3+}$	261.8(60) *240.9*	259.1(60) *238.2*	258.4(20)	263(4)	n/o	251.8(2)	148.8(5) *227.9*
$[LM(CO_3)ClO_4)]^{+}$	885.5(5)	875.3(5)	875.4(5)	889.3(2)	845.0(2)	860.1 [c]	845.4(5)
$[LM(HCO_3)(ClO_4)]^{2+}$	443.1(20)	438.1(50)	438.1(5)	444.3(2)	n/o	n/o	423.0(10)
$[LM(HCO_3)(ClO_4)_2]^{+}$	985.3(5)	975.2(5)	975.5(5)	989.2(0.2)	[c]	n/o	945.2(5)

[a] Odense results, except where indicated. [b] Swansea results (20 V cone voltage). [c] Very weak; fractional percentage intensity.

Table 5 Ions (*m*/*z* values for the major isotopomer of the cluster) observed in the ESI mass spectra of the methylcarbonate complexes

Cryptate	$[M_2L^1(MeCO_3)(ClO_4)]^{2+}$	$[M_2L^1(MeCO_3)(ClO_4)_2]^{+}$
$[Cu_2L^1(MeCO_3)](ClO_4)_3$ **2**	450.1	999.9
$[Zn_2L^1(MeCO_3)](ClO_4)_3$ **10**	442.2	1003.5
$[Co_2L^1(MeCO_3)](ClO_4)_3$ **6**	445.2	989.3

ation. We have previously found that a diiron and a dicopper complex containing a μ-η¹,η¹-CO_3^{2-} group (mode ***C***) lose the mass equivalent to CO_2 under CA to generate unusual dinuclear oxide complexes.[37] The present series of carbonate complexes offers an opportunity to compare the gas-phase fragmentation of alternative carbonate bonding modes as well as the effect of encapsulation within a cryptand ligand. CA of the $[M_2L^1(CO_3)]^{2+}$ and $[M_2L^1(HCO_3)]^{3+}$ ions produced only one daughter ion due to the loss of a mass equivalent to carbonic acid (H_2CO_3). Thus the $[M_2L^1(CO_3)]^{2+}$ and $[M_2L^1(HCO_3)]^{3+}$ ions generate the $[M_2(L^1 - 2H)]^{2+}$ and $[M_2(L^1 - H)]^{3+}$ ions, respectively (Fig. 8(a) and (b)). It has recently been demonstrated that carbonic acid has reasonable gas phase stability and is capable of sublimation.[38,39] We suggest that the presence of the secondary amine groups in the cryptand ligands favour this decomposition pathway in comparison to the above-mentioned diiron and dicopper complexes which did not contain secondary amine ligands in their coordination spheres. Although this fragmentation pathway is an interesting confirmation of H_2CO_3 gas-phase stability its generality means that we are unable to differentiate the various carbonate bonding modes using mass spectrometry.

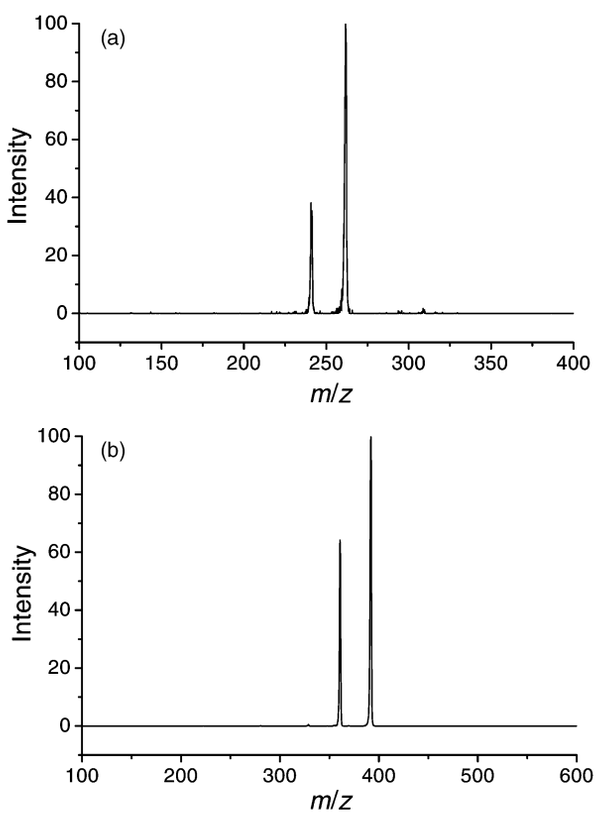

Fig. 8 Collision activation experiment for (a) μ-carbonato dicopper cryptate peak and (b) the analogous μ-hydrogencarbonato dicopper peak.

An interesting observation was that higher pressures of Ar were required to produce the daughter ions in the case of the nickel and cobalt complexes compared to the copper and zinc complexes, Fig. 9. This reflects a tendency to favour the octahedral environment which is expected to generate greater stability for Co and Ni complexes in comparison with Cu and Zn analogues. To our knowledge an effect of this nature has not previously been reported.

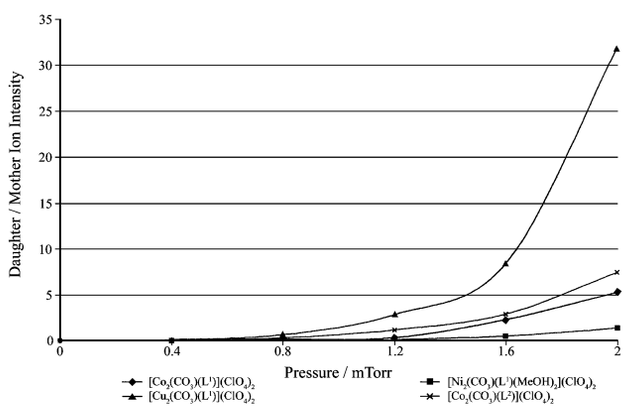

Fig. 9 Intensity of collision-activation generated product $(M_2L^1 - 2H^+)^{2+}$ as a function of argon pressure in the series of dinuclear μ-carbonato cryptates.

The spectra for the three methyl carbonate species are simple and show the corresponding ion pair and triplet, $[M_2L^1(MeCO_3)(ClO_4)]^{2+}$ and $[M_2L^1(MeCO_3)(ClO_4)_2]^{+}$ (Table 5). Relative intensities are not included in the table since conditions could be varied to give either the doubly- or singly-charged ion as base peak. Minor peaks due to the loss of methyl radical and methoxy radical are evident in the spectra of the cobalt and copper complexes.

Conclusion

The similar host molecules L^1 and L^2 show different behaviour in the "cascade" generation of $MeCO_3^-$ *via* CO_2 insertion into the OMe^- bond; a reaction which is facile within L^1, but which fails to take place at an observable rate within L^2. Part of the responsibility for this failure may lie in the efficient coordination of alkoxo within the effectively smaller cavity of L^2; the colinear M–O(Me)–M assembly inferred by analogy with structurally characterised dicopper(II) and dizinc(II) μ-hydroxo cryptates is presumably subject to thermodynamic stabilisation, which together with inappropriate geometry explains the absence of CO_2 insertion reaction within L^2.

The facile generation of monomethyl carbonate in the catalysed reaction may have implications for the polymer industry, as it indicates a potentially useful route to unsymmetric carbonate esters.

The hosts also show different preference for bridging carbonate modes; the more compact L^2 cavity encouraging the single-atom bridging μ-η_2,η_2 mode over the variety of μ-η_1,η_1 and μ-η_1,η_2 modes adopted within L^1. The different bridging modes are reflected in different mediation of magnetic interactions; the most efficient mediation being observed in the μ-η_2,η_2 mode favoured within L^2.

ESI-MS studies show ready loss of carbonic acid in the carbonato-bridged cryptates and of methyl and methoxy radicals in the methylcarbonate-bridged cryptates. No dependence of CA behaviour on mode of bridging could be discerned.

Experimental

Synthesis of cryptates

The free ligands L^1 and L^2 were synthesised as described earlier.[19,40] **CAUTION:** Many of these cryptates contain perchlorate counter-ion, which represents a known explosion hazard and so must be handled with care. However under the circumstances described here, we experienced no problems.

Carbonate syntheses

The metal salt $M(ClO_4)_2 \cdot xH_2O$, 0.2 mmol, in 8 cm^3 of a 1 : 1 EtOH–MeCN mixture was added to 0.1 mmol of the cryptand L^1 or L^2 in 5 cm^3 EtOH and stirred for 5 min before adding 0.1 mmol Na_2CO_3 dissolved in 1–2 cm^3 H_2O. The solution was then left to evaporate in air or under CO_2 atmosphere before filtration to yield a microcrystalline product which was recrystallised from MeCN or MeCN–alcohol using diethyl ether diffusion to generate suitable crystals for X-ray crystallography; **3** and **5** were recrystallised from MeCN–MeOH.

In the case of the zinc(II) and copper(II) complexes, there was a tendency for μ-hydroxo complexes to crystallise out together with μ-carbonato complexes, and the proportion of hydroxo impurity increased on recrystallisation. Although the reported crystal structure, **11**, was unambiguously that of a carbonate, the microanalytical data for the bulk sample of dizinc μ-carbonato cryptate were unsatisfactory for that formulation, suggesting a large percentage of hydroxo impurity.

Yields (following recrystallisation): 20–40%. Colours: **1** green, **3** blue, **5** olive-green, **7**, blue–green, **8** olive-green, **9**, **11** cream–white.

Methylcarbonate syntheses

To 0.1 mmol L^1 in 8 cm^3 MeOH was added 0.2 mmol $M(ClO_4)_2 \cdot xH_2O$ dissolved in 5 cm^3 1 :1 MeOH–MeCN. Any instantaneous amorphous precipitate was redissolved by adding MeCN and the solution allowed to evaporate in air followed by slow MeOH diffusion until crystals were obtained. Yields (after recrystallisation): 30–50%. Colours: **2** peacock-blue, **4** aqua-blue, **6**, olive-green, **10**, white.

When this procedure was repeated for L^2 and Co(II) or Ni(II), no solid products were obtained on standing for many days, however on addition of preformed carbonate anion rapid crystallisation of carbonate-bridged cryptate **8** or **9** ensued.

ESI-MS

Mass spectral data for the carbonate and hydrogencarbonate complexes were recorded on a Finnigan TSQ 700 MAT triple quadrupole instrument equipped with a nanoelectrospray source.[41] Spectra were obtained by spraying an acetonitrile solution from a Au/Pd coated needle held at 0.7 kV and introduced to the mass spectrometer through the capillary tube heated to 150 °C and at a potential of 20 V. Sample concentrations were typically 0.3 mM. CID experiments were performed typically employing a 0.5–1 mTorr argon pressure in the collision cell. The region from *m*/*z* 100 to 1000 was scanned for 2 s and the spectra were obtained by averaging 60 scans. The mass spectra of the methyl carbonate complexes were recorded using an ION SPEC FTICR.

Magnetic measurements

Variable-temperature magnetic measurements were carried out on polycrystalline samples using a Faraday type magnetometer (Oxford Instruments), equipped with a helium continuous-flow cryostat working in the temperature range 280–4 K, and an electromagnet operating at a magnetic field of 0.8 T. Diamagnetic corrections were estimated from Pascal's Tables.

Magnetic data were recorded for each of the complexes **1**–**8** over the approximate temperature range 4–280 K. Fitting plots and raw data are included in the supplementary information (ESI). † In each case the data were fitted to the isotropic expression[42] (eqn. (1)) for the temperature-variation of magnetic susceptibility for the appropriate spin state by minimising the *R* factor: $(R = \Sigma\{(\chi_m T)_{calc} - (\chi_m T)_{exptl})^2/(\chi_m T)_{exptl}]^2)$.

$$H = -J_1 S_1 S_2 \quad (1)$$

A temperature-independent contribution was included for each complex (see Table 3), and for complexes **1** and **7** a paramagnetic impurity term was included in the fitting procedure (see Table 3). These were evaluated as 6% for **1** and 1.8% for **7**. In line with the intermolecular hydrogen-bonded structure of **1**, inclusion of a molecular field term, $\theta = -0.7$ K, gave rise to a slight increase in the estimated impurity (7%) and no significant change in *J*. The best fit values of *g* that were evaluated for **1** are lower than to be expected for copper complexes. Imposing a higher *g* value in the fitting routine resulted in significantly worse fitting but with slightly larger coupling constant; if *g* is fixed at 2.1, $-J$ is 240 cm^{-1}.

In the absence of an exact analytical function for describing the exchange interaction in dimeric cobalt complexes with the inclusion of spin–orbit effects, we have fitted the data using spin-only equations. Interpretation of the data for complex **5** is further complicated by the existence of two cations of different structure in the unit cell. In accord with this structure, the data for complex **5** were least-squares fitted to an expression for the magnetic susceptibility based on an equimolar mixture of two pairs of independently interacting dinuclear ions with independent *g* values and intramolecular exchange parameters J_1 and J_2 (eqn. (2)). Evaluation of five parameters (g_1, J_1, g_2, J_2 and TIP) from a data set in which the susceptibility does not reach a maximum value is likely to lead to large uncertainty in these terms, although this is not reflected in the error limits generated on these parameters (see Table 3).

$$H = -(0.5J_1 S_1 S_2 + 0.5J_2 S_1 S_2) \quad (2)$$

The larger of the *J* values is assigned to the mode ***B*** and is consistent with dicopper systems in which this mode operates.

In the case of identical bridging geometry the product n^2J, where n is the number of unpaired electrons on the paramagnetic centre, is expected[35] to be constant. The assignment of the stronger coupling constant to mode ***B*** is thus supported by comparison with a square-based dicopper complex, for which a J value of -125 cm^{-1} is reported,[2] approximately 9 ($= n^2$) times that observed for this dicobalt system.

The magnetic behaviour of complex **8** is complex, but is reproduced in studies of two separate syntheses, both of which yielded crystalline products, which appeared homogeneous on microscopic examination. As the temperature is lowered, the susceptibility rises to a maximum in the region of 70 K before flattening and rising again (Fig. 10). While the data in the high-

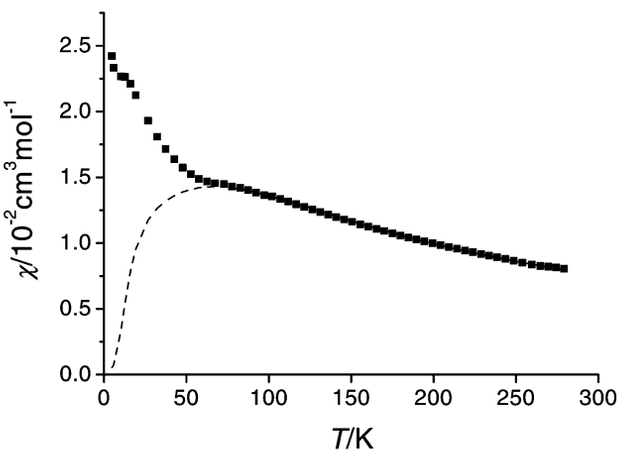

Fig. 10 Magnetic behaviour (χ *vs.* T) for complex **8** showing the close fit of the data to the parameters in Table 3 over the temperature range 70–280 K. Below 70 K the data diverges from the prediction of the Heisenberg model (dashed line).

temperature regime (70–280 K) may be fitted closely to a moderately strong antiferromagnetic exchange (Table 3), the low temperature behaviour is puzzling and we are unable to find a convincing explanation for it. Attempts to fit the data to a model including impurity or spin crossover effects were unsuccessful. An alternative rationalisation for the behaviour of **8** could be the onset of a phase change to a more weakly coupled bridging of the Co(II) ions. The occurrence of two bridging modes in complex **5** suggests that a fine balance indeed exists between favoured coordination modes of carbonate in these systems.

X-Ray crystallography

Data for complexes **1**, **5**, and **8** were collected on a Siemens SMART 1K diffractometer; complexes **2** and **10** were collected on line 9.8 of the SRS, Daresbury; complexes **3** and **4** were collected on a Siemens P4 diffractometer and complex **11** was collected on a Bruker SMART 1000. Details of the data collections and refinements are given in Table 6. The structures were all solved by direct methods and refined by full-matrix least-squares on F^2, using SHELXTL.[43] Except where otherwise stated below, all non-hydrogen atoms were refined with anisotropic atomic displacement parameters. Hydrogen atoms bonded to carbon or nitrogen were inserted at calculated positions with isotropic displacement parameters riding on U_{ij} of their carrier atoms; hydrogen atoms bonded to oxygen were located from difference Fourier maps and not further refined.

CCDC reference numbers 181027–181034.

See http://www.rsc.org/suppdata/dt/b1/b110449g/ for crystallographic data in CIF or other electronic format.

$[Cu_2(L^1)(CO_3)](ClO_4)_2\cdot 2H_2O$, $C_{37}H_{64}Cl_2Cu_2N_8O_{13}$ (1). The structure was refined as described above, there is no disorder.

Table 6 X-Ray data

	1	2	3	4	5	8	10	11
Empirical formula	$C_{37}H_{64}Cl_2Cu_2N_8O_{13}$	$C_{41.60}H_{68.40}Cl_3Cu_2N_{8.60}O_{17.40}$	$C_{39.50}H_6Cl_2N_8Ni_2O_{14}$	$C_{41.50}H_{62.25}Cl_3N_{9.75}Ni_2O_{15}$	$C_{74}H_{120}Cl_4Co_4N_{16}O_{25}$	$C_{31}H_{50}Cl_2Co_2N_8O_{15}$	$C_{40}H_{62.50}Cl_3N_{8.50}O_{16}Zn_2$	$C_{37}H_{67}Cl_2N_8O_{17.50}Zn_2$
Formula weight	1026.94	1200.88	1064.32	1161.53	2011.38	963.55	1155.58	1105.63
Temperature/K	158(2)	153(2)	153(2)	150(2)	162(2)	169(2)	150(2)	150(2)
Wavelength/Å	0.71073	0.48480	0.71073	0.71073	0.71073	0.71073	0.68850	0.71073
Crystal system	Orthorhombic	Monoclinic	Orthorhombic	Monoclinic	Orthorhombic	Triclinic	Orthorhombic	Triclinic
Space group	*Pbca*	$P2_1/n$	$Pca2_1$	$P2_1/n$	$Pna2_1$	$P\bar{1}$	*Pccn*	$P\bar{1}$
a/Å	19.195(3)	12.4559(5)	24.320(3)	16.790(3)	21.5207(11)	11.870(6)	27.9616(15)	12.7298(6)
b/Å	17.909(3)	30.8743(13)	10.8310(16)	17.247(3)	21.7232(11)	12.320(6)	33.7851(17)	13.8296(7)
c/Å	24.650(4)	13.8395(6)	19.546(2)	19.352(3)	20.0882(10)	16.954(9)	10.9883(5)	14.6010(7)
α/°	90	90	90	90	90	71.358(7)	90	74.817(1)
β/°	90	105.039(1)	90	112.757(12)	90	74.496(7)	90	81.738(1)
γ/°	90	90	90	90	90	88.330(8)	90	75.403(1)
V/Å^3	8474(2)	5139.9(4)	5148.5(11)	5167.5(15)	9391.2(8)	2259.4(19)	10380.5(9)	2392.4(2)
Z	8	4	4	4	4	2	8	2
μ/mm^{-1}	1.205	0.561	0.901	0.957	0.886	0.921	1.151	1.193
Refl. collected	48784	37650	4533	6962	59921	14824	17593	17593
Indep. refl. [*R*(int)]	6520 [0.0666]	12995 [0.0453]	4308 [0.0375]	6694 [0.0427]	14563 [0.0682]	7018 [0.0885]	9961 [0.0542]	8406 [0.0358]
*R*1, *wR2* [$I > 2\sigma(I)$]	0.0330, 0.0792	0.0660, 0.1392	0.0592, 0.1255	0.0814, 0.1891	0.0776, 0.2035	0.1156, 0.3298	0.0721, 0.2073	0.0425, 0.1130
*R*1, *wR2* (all data)	0.0577, 0.0841	0.0880, 0.1448	0.0994, 0.1461	0.1621, 0.2332	0.0986, 0.2220	0.2035, 0.3724	0.1084, 0.2271	0.0584, 0.1201

$[Cu_2(L^1)(MeCO_3)](ClO_4)_3\cdot 2.4MeOH\cdot 0.6MeCN$, $C_{41.60}H_{68.40}Cl_3Cu_2N_{8.60}O_{17.40}$ (2). The cation is fully ordered but two of the perchlorate anions are disordered and the solvate acetonitrile is disordered 60 : 40 with a methanol molecule at the same site. The hydrogen atoms on the methanol molecules were not located or included in the model.

$[Ni_2(L^1)(CO_3)(MeOH)_2](ClO_4)_2\cdot 0.5MeOH\cdot 0.5H_2O$, $C_{39.50}H_6Cl_2N_8Ni_2O_{14}$ (3). No disorder, although the non-coordinated solvate methanol and water molecules were refined with 50% site occupancy. The hydrogen atoms of the water molecule were not located or included in the model.

$[Ni_2(L^1)(MeCO_3)(MeOH)_2](ClO_4)_3\cdot 1.75MeCN$, $C_{41.50}H_{62.25}Cl_3N_{9.75}Ni_2O_{15}$ (4). The methylcarbonate anion is disordered 60 : 40 over the two equivalent *syn–anti* coordination sites bridging the nickel ions. Possibly as a consequence of this, the saturated sections of one of the strands of the cryptate ligand is also disordered 60 : 40 between two related positions. One of the three perchlorate ions is ordered, one shows a 60 : 40 disorder over two positions related by rotation about one of the Cl–O bonds, and the third has been modelled as split over four overlapping positions (40 : 30 : 20 : 10). One MeCN was modelled with 75% occupancy.

$[Co_2(L^1)(CO_3)][Co_2(L^1)(CO_3)(H_2O)_2](ClO_4)_4\cdot 2H_2O$, $C_{74}H_{120}Cl_4Co_4N_{16}O_{25}$ (5). This structure contains two independent (and different) cations, each with disorder about one amine in the saturated section of one strand. One of the water molecules is disordered over two positions and one perchlorate anion shows disorder over two positions related by rotation about one of the Cl–O bonds. All of these have been modelled with 50% occupancy of each site. The hydrogen atoms bonded to water were not located and have not been included in the refinement.

$[Co_2(L^2)(CO_3)](ClO_4)_2\cdot H_2O$, $C_{31}H_{50}Cl_2Co_2N_8O_{15}$ (8). One perchlorate anion shows disorder (55 : 46) over two positions related by rotation about one of the Cl–O bonds. The hydrogen atoms bonded to water were not located and have not been included in the refinement.

$[Zn_2(L^1)(MeCO_3)](ClO_4)_3\cdot MeOH\cdot 0.5MeCN$, $C_{40}H_{62.50}Cl_3N_{8.50}O_{16}Zn_2$ (10). The methylcarbonate anion is disordered 75 : 25 over the two equivalent *syn–anti* coordination sites bridging the zinc ions. Two of the perchlorate anions are disordered, one is disordered over two positions (60 : 40), sharing two of the oxygen sites while the other shows disorder over two positions related by rotation about one of the Cl–O bonds (50 : 50). Two molecules of methanol and one of acetonitrile have been refined at 50% site occupancy; no hydrogen atoms have been inserted for these solvates.

$[Zn_2(L^1)(CO_3)](ClO_4)_2\cdot 6.5H_2O$, $C_{37}H_{67}Cl_2N_8O_{17.50}Zn_2$ (11). The cation is fully ordered. One of the perchlorate anions is disordered (67 : 33) over two sites sharing three of the oxygen sites. The lattice contains three full-occupancy water molecules; additional lattice water molecules have been inserted at 50% occupancy in six positions and at 25% occupancy in two positions. No hydrogen atoms have been included for the partial occupancy molecules.

Acknowledgements

We wish to thank EPSRC for access to the Mass Spectroscopy service at Swansea and to Station 9.8 at Daresbury Laboratory. We are grateful to OURC for support (to Y. D.) as well as to the Danish Natural Science research council (CJM) for Grant no. 28808. We thank Bogdan Budnik for recording the mass spectra of the methylcarbonate complexes.

References

1 F. Botre, G. Grows and B. T. Storey, *Carbonic Anhydrase*, VCH Weinheim, 1991.
2 A. Escuer, F. A. Mautner, E. Penalba and R. Vicente, *Inorg. Chem.*, 1998, **37**, 4190.
3 A. Farooq, R. R. Jacobsen, K. D. Karlin, P. P. Paul, Z. Tykelar and J. Zubieta, *J. Am. Chem. Soc.*, 1989, **111**, 388.
4 A. Dworkin, H. Hope, M. Julve, O. Kahn, J. Sletten and M. Verdaguer, *Inorg. Chem.*, 1988, **27**, 542.
5 B. Dietrich, J. Guilhem, J.-M. Lehn, C. Pascard and E. Sonveaux, *Helv. Chim. Acta*, 1984, **67**, 91; B. Dietrich, M. W. Hosseini, J.-M. Lehn and R. B. Sessions, *Helv. Chim. Acta*, 1983, **66**, 1262.
6 M. Hynes, B. Maubert, J. Nelson, V. McKee and R. M. Town, *J. Chem. Soc., Dalton Trans.*, 2000, 2853.
7 C. J. Harding, F. J. Mabbs, E. J. MacInnes, V. McKee and J. Nelson, *J. Chem. Soc., Dalton Trans.*, 1996, 3227.
8 A. Escuer, C. J. Harding, Y. Dussart, J. Nelson, V. McKee and R. Vicente, *J. Chem. Soc., Dalton Trans.*, 1999, 223.
9 J.-M. Lehn, *Pure Appl. Chem.*, 1980, **52**, 2441; J.-M. Lehn, *Science*, 1985, **227**, 849.
10 A. G. Shaikh and S. Sivaram, *Chem. Rev.*, 1996, **96**, 951.
11 L. Fabrizzi, P. Pallavicini, L. Parodi and A. Taglietti, *Inorg. Chim. Acta*, 1995, **238**, 5.
12 Y. Dussart, C. J. Harding, V. McKee and J. Nelson, *Inorg. Chim. Acta*, in preparation.
13 N. Kitajima, S. Hikichi, M. Tanaka and Y. Moro-Oka, *J. Am. Chem. Soc.*, 1993, **115**, 5496 and references therein.
14 C. J. Harding, Q. Lu, V. McKee and J. Nelson, *J. Chem. Soc., Chem. Commun.*, 1993, 1768.
15 R. L. Rardin, W. B. Tolman and S. J. Lippard, *New J. Chem.*, 1991, **15**, 417.
16 R. L. Rardin, P. Poganiuch, A. Bino, D. P. Goldberg, W. B. Tolman, S. C. Liu and S. J. Lippard, *J. Am. Chem. Soc.*, 1992, **114**, 5240.
17 D. A. Palmer and R. Van Eldik, *Chem. Rev.*, 1983, 651.
18 S. C. Rawle, C. J. Harding, P. Moore and N. W. Alcock, *J. Chem. Soc., Chem. Commun.*, 1992, 1701.
19 C. J. Harding, Q. Lu, J. F. Malone, D. J. Marrs, N. Martin, V. McKee and J. Nelson, *J. Chem. Soc., Dalton Trans.*, 1995, 1739.
20 V. C. Arunasalam, I. Baxter, J. A. Darr, S. R. Drake, M. B. Hursthouse, K. M. A. Malik and D. M. Mingos, *Polyhedron*, 1998, **641**, 17.
21 M. R. Churchill, G. Davies, M. A. ElSayed, M. F. El-Shalzy, J. P. Hutchinson and M. W. Rupich, *Inorg. Chem.*, 1980, **19**, 201 and references therein.
22 J. Nelson and V. McKee, to be published.
23 K. Nakamoto, *IR and Raman Spectra of Inorganic and Coordination Compounds*, John Wiley and Sons, New York, 4th edn., 1986.
24 B. M. Gatehouse, S. E. Livingston and R. S. Nyholm, *J. Chem. Soc.*, 1958, 3137.
25 D. Ballivet-Tkatchenko, O. Doteau and S. Stutzmann, *Organometallics*, 2000, **19**, 4563.
26 G. R. Deacon and R. J. Philips, *Coord. Chem. Rev.*, 1980, **33**, 227.
27 A. Escuer, R. Vicente, S. B. Kumar, X. Solans and M. Font-Bardia, *J. Chem. Soc., Dalton Trans.*, 1997, 403.
28 A. Escuer, R. Vicente, S. B. Kumar, X. Solans, M. Font-Bardia and A. Caneschi, *Inorg. Chem.*, 1996, **35**, 3094.
29 A. L. Brenk, K. A. Byriel, D. P. Fairlie, L. R. Gahan, G. R. Hanson, C. J. Hawkins, A. Jones, C. H. L. Kennard, B. Moubaraki and K. S. Murray, *Inorg. Chem.*, 1994, **33**, 3549 and references therein.
30 CACAO Program: C. Mealli and D. M. Proserpio, *J. Chem. Educ.*, 1990, **67**, 399.
31 A. Escuer, M. S. El-Fallah, S. B. Kumar, F. Mautner and R. Vicente, *Polyhedron*, 1999, **18**, 377 and references therein.
32 H. Harada, M. Kodera, G. Vuckovic, N. Matsumoto and S. Kida, *Inorg. Chem.*, 1991, **30**, 1190.
33 A. Escuer, R. Vicente, E. Penalba, X. Solans and M. Font-Bardia, *Inorg. Chem.*, 1996, **35**, 248.
34 E. Colacio, M. Ghazi, R. Kivekas and J. M. Moreno, *Inorg. Chem.*, 2000, **39**, 2882.
35 O. Kahn, *Molecular Magnetism*, Wiley-VCH, New York, 1992.
36 U. N. Andersen, C. J. McKenzie and G. Bojesen, *Inorg. Chem.*, 1995, **34**, 1435.
37 P. Dalgaard and C. J. McKenzie, *J. Mass Spectrom.*, 1999, **34**, 1033.
38 T. Loerting, C. Tautermann, R. T. Kroemer, I. Kohl, A. Hallbrucker, E. Mayer and K. K. R. Liedl, *Angew. Chem., Int. Ed.*, 2000, **39**, 891.
39 R. Ludwig and A. Kornath, *Angew. Chem., Int. Ed.*, 2000, **39**, 1421.
40 Q. Lu, J. M. Latour, C. Harding, N. Martin, D. Marrs, V. McKee and J. Nelson, *J. Chem. Soc., Dalton Trans.*, 1994, 1471.
41 M. Wilm and M. Mann, *Anal. Chem.*, 1996, 681.
42 C. J. O'Connor, *Prog. Inorg. Chem.*, 1982, **29**, 203.
43 G. M. Sheldrick, SHELXTL Version 5.1, Bruker AXS, Madison, WI, 1998.